Solvent-Free Synthesis and Processing of Conductive Elastomer Composites for Green Dielectric Elastomer Transducers

Patrick M. Danner, Mihail Iacob, Giacomo Sasso, Iurii Burda, Bernhard Rieger, Frank Nüesch, and Dorina M. Opris*

Stretchable electrodes are more suitable for dielectric elastomer transducers (DET) the closer the mechanical characteristics of the electrodes and elastomer are. Here, a solvent-free synthesis and processing of conductive composites with excellent electrical and mechanical properties for transducers are presented. The composites are prepared by in situ polymerization of cyclosiloxane monomers in the presence of graphene nanoplatelets. The low viscosity of the monomer allows for easy dispersion of the filler, eliminating the need for a solvent. After the polymerization, a cross-linking agent is added at room temperature, the composite is solvent-free screen-printed, and the cross-linking reaction is initiated by heating. The best material shows conductivity $\sigma = 8.2$ S cm^{-1}, Young's modulus $Y_{10\%} = 167$ kPa, and strain at break $s = 305\%$. The electrode withstands large strains without delamination, shows no conductivity losses during repeated operation for 500 000 cycles, and has an excellent recovery of electrical properties upon being stretched at strains of up to 180%. Reliable prototype capacitive sensors and stack actuators are manufactured by screen-printing the conductive composite on the dielectric film. Stack actuators manufactured from dielectric and conductive materials that are synthesized solvent-free are demonstrated. The stack actuators even self-repair after a breakdown event.

1. Introduction

There is an increasing need for environmentally friendly stretchable conductors that can be easily applied on different substrates without damaging the underlying substrate. Such electrode materials are urgently searched for the growing fields of stretchable electronics and dielectric elastomer transducers (DET).

DETs change shape in response to an electric field, generate electricity when stretched, and sense a change caused by a mechanical load through the change in capacitance.[1–6] It is essential that the different moving parts upon action remain as a coherent unit and do not delaminate despite an "infinite" number of mechanical stretching and electrical charging during device operation.[7–11] The electrodes allow charging and discharging of the capacitor. During DET operation, the electrodes and the dielectric are deformed to the same extent. Therefore, their compliance and mechanical properties are crucial for transducers' lifetime and performance. The change in conductivity with strain and the number of cyclic strains it can sustain unchanged is also important. Often, only the conductivity at different uniaxial strain levels is reported for new electrode materials. However, a low change in conductivity with strain is insufficient for a conductive material to qualify as a promising electrode material for DET. It is thus also important to evaluate the conductivity under a biaxial strain and assess an electrodes' performance under repetitive

P. M. Danner, M. Iacob, G. Sasso, F. Nüesch, D. M. Opris
Swiss Federal Laboratories for Materials Science and Technology Empa
Laboratory for Functional Polymers
Ueberlandstr. 129, Dübendorf CH-8600, Switzerland
E-mail: dorina.opris@empa.ch

P. M. Danner, B. Rieger
Wacker-Chair of Macromolecular Chemistry
Catalysis Research Center, Department of Chemistry
Technical University of Munich
Garching 85748, Germany

P. M. Danner
Department of Materials
ETH Zürich
Vladimir-Prelog-Weg 5, Zurich CH-8093, Switzerland

I. Burda
Swiss Federal Laboratories for Materials Science and Technology Empa
Laboratory for Mechanical Systems Engineering
Ueberlandstr. 129, Dübendorf CH-8600, Switzerland

F. Nüesch
Ecole Polytechnique Fédérale de Lausanne (EPFL)
Institut des Matériaux
Station 12, Lausanne CH-1015, Switzerland

ADVANCED
SCIENCE NEWS
www.advancedsciencenews.com

Macro-
molecular
Rapid Communications
www.mrc-journal.de

stretching at high voltages. For instance, Shea et al. have found that when the electrodes are stretched above 20% upon DET actuation, significant damages occur after a few thousand cycles, and the actuation turns inhomogeneous.[12] The same group compared different carbon-based electrodes and found that the aging of actuators depends on the overall actuation time and is independent of the frequency.[13] Additionally, the viscoelasticity of electrodes and the ramping rate of applied triangular voltages were found to influence the actuation.[14] The stability of the electrode under high voltages is another concern in actuator and generator applications.

Stretchable electrodes for DETs are commonly made by applying conductive inks on stretchable substrates or by making composites of conductive fillers in elastic matrices.[15] For instance, suspensions of conductive fillers such as carbon, conductive polymers, carbon nanotubes (CNT), Ag and Cu nanowires, Ag flakes in a solvent or composites of conductive fillers in elastic matrices have been extensively explored.[15–23]

Although CNTs and metal nanowires (NWs) provide great conductivity, compliance, stability under high voltages, and may self-clear, these materials are not without drawbacks.[24–26] The former is cancerogenic, while the latter is rather expensive and needs large amounts of solvents for its synthesis.[27,28] Doped conductive polymers such as poly(3-dodecyloxylthiophene) and polyaniline showed promising conductivity.[29,30] However, the high voltage instability and high Young's modulus make them unsuitable for actuator and generator applications.[26,29]

The most explored electrode materials for transducers are based on carbonaceous fillers. Shea et al. used 10 wt% of carbon black (CB) in commercial polydimethylsiloxane (PDMS) and pad-printed it to electrodes with a thickness of roughly 4–8 µm and resistance around 300–100 kΩ, respectively.[2,12,31] Peng et al. used single-wall carbon nanotubes (SWCNT) electrodes and obtained self-clearable electrodes with a sheet resistance of 100 kΩ sq^{-1} and good stability over one thousand cycles at an areal actuation strain of 150%.[25] Quinsaat et al. used a mixture of carbon black and graphene nanoparticles (GNPs) dispersed in a PDMS and achieved an electrode material with a conductivity of 7.8 S cm^{-1} and contact resistance of 5 Ω.[32] The electrode was processed by screen-printing, which was facilitated by adjusting the viscosity of the composite by solvent. More recently, it has been shown that liquid metals dispersed in a PDMS matrix allowed the formation of elastic electrodes with a low starting sheet resistance below 0.1 Ω sq^{-1}, a Young's modulus of 500 kPa, and a strain at break of 700%.[33–35] Additionally, the electrode withstood voltages of up to 9 kV and showed only a slight increase in resistance with stretching. Liquid metals, however, have their limitations, including cost, high density, oxidation, and aging.

For actuator applications, the electrode material should not stiffen the device. Thus, its Young's modulus should be low.[12,15,26] However, conductive fillers increase the Young's modulus of a composite, often to a few MPa, which is way too much for many applications. To mitigate this problem, the electrode thickness can, in principle, be decreased.[12] However, this strategy also has limitations, as thinner electrodes show higher resistance and require sophisticated processing techniques. One of the thinnest actuators consists of a 1.4 µm thick dielectric layer with a 2 nm thin electrode by Ji et al. 2018.[26] The electrod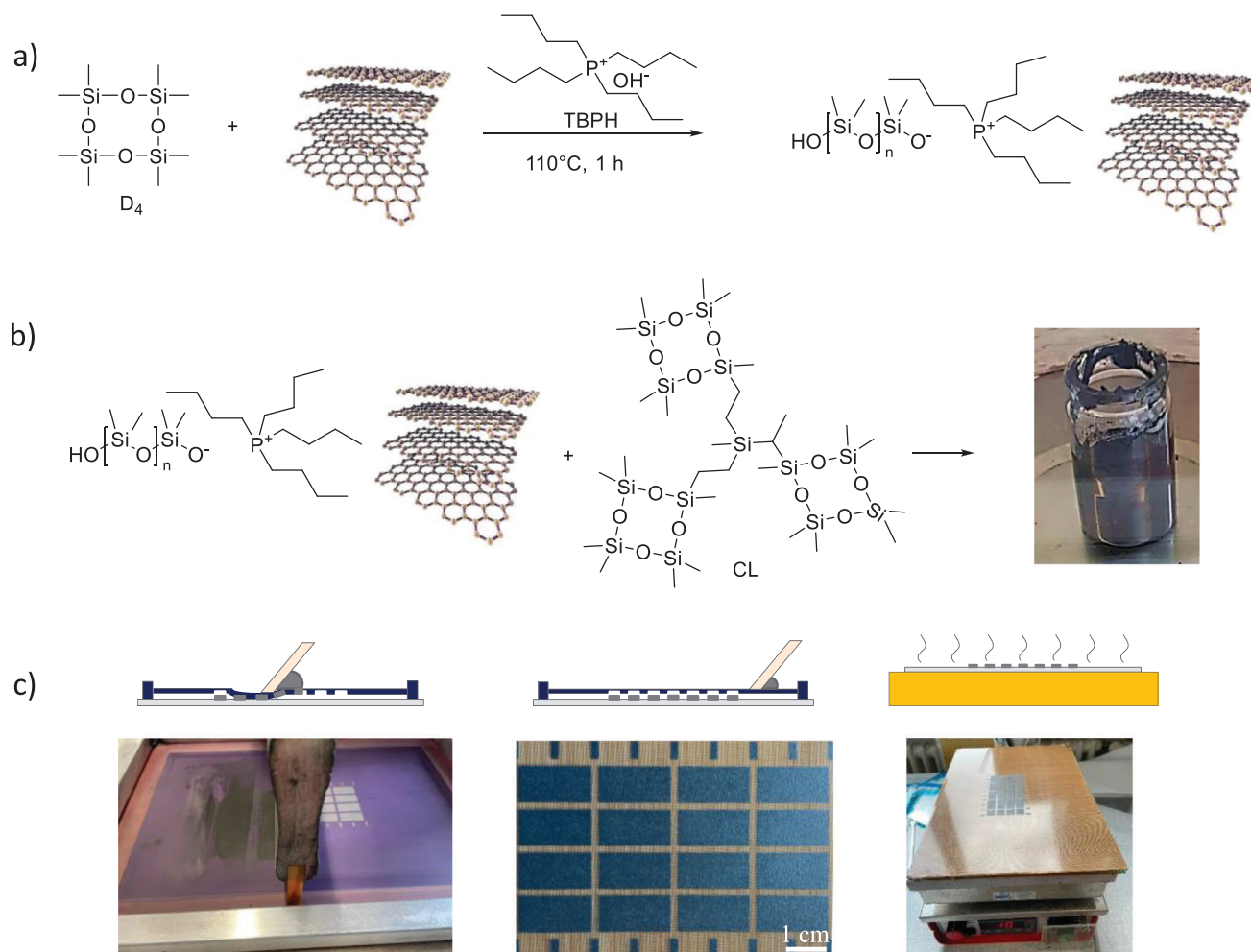e Young's modulus was estimated as 37 MPa and showed a sheet resistance of 20 MΩ sq^{-1}, which is rather high. Another possibility is to use soft hydrogels as an electrode.[36] However, their performance and stability are significantly lower compared to composite electrode materials. Soft conductive composites based on carbon fillers in a PDMS matrix were reported by Bele et al. and Michel et al.[37,38] Both groups obtained composites with an elastic modulus of 280 kPa and used them as electrodes in actuators. This was indeed a significant reduction in Young's modulus but still, a solvent was needed to enable processability into thin films by adjusting the viscosity of the composite. Solvent addition allows adjusting the viscosity of the composite to be printed at will. However, it's major drawback, besides the negative environmental impact, is swelling the underneath dielectric layer on which it is printed, producing defects. Such defects will significantly reduce device lifetime and complicate the processing of multiple layered devices.

In addition to the electrical and mechanical properties, the electrode material's accurate application impacts the final device's performance and lifetime, especially when stack actuators are envisioned. Electrodes are typically applied by 3D printing,[39] spray coating,[40] inkjet printing,[41] laser ablation,[2] and screen-printing.[42] Filamentary printing of vertically oriented electrodes was demonstrated with an 18 wt% carbon black in polyethylene glycol PEG-PES oligomer solution.[39] However, a significant synthetic effort had to be invested to achieve a composite with the desired properties for printing. Concerning spray coating and inkjet printing, tedious work is required to find optimal printing conditions for each ink and substrate. Additionally, the ink can clog the needle and expensive equipment is needed. High-resolution electrodes with excellent design flexibility were made by laser ablation of a blade-coated composite of 10 wt% carbon black in a PDMS matrix. The electrodes were subsequently bonded to a PDMS membrane by oxygen plasma activation.[2] Actuators with an area strain of over 25% and interdigitated capacitive touch sensors with high sensitivity were demonstrated. Although this is a simple way to manufacture devices and allows easy production of laboratory prototypes, the process is difficult to be scaled up.

Screen printing is widely used in printed electronics.[43,44] It produces little waste and is cheap and straightforward. It allows different printing patterns with resolutions as high as 30–50 µm.[43,45] However, the accuracy of this printing technique is highly dependent on the properties of the conductive ink used.[45]

Thus, the major drawbacks of currently reported electrode materials include high Young's Modulus, delamination and degradation during operation, and last but not least, the need to use solvent for processing. A solvent-free synthesis and processing of electrode material is environmentally friendly and has processing advantages in layer-by-layer printing of different materials, where solvent often interferes with the printed layers.

Here, conductive silicone composites are developed starting from monomers. Both, their synthesis and manufacturing by screen-printing are solvent-free. To achieve this, we used anionic polymerization of octamethylcyclotetrasiloxane monomer (D$_4$) at elevated temperatures in the presence of GNP filler. A multifunctional cyclosiloxane monomer cross-linker is added to the resulting composite at room temperature. The composites are processed by screen-printing and then cross-linked by heating to elevated temperatures. The elastic properties can be fine-tuned by the amount of initiator and multifunctional cross-linker used.

ADVANCED
SCIENCE NEWS
www.advancedsciencenews.com

[M]acro-
molecular
Rapid Communications
www.mrc-journal.de

Figure 1. The steps involved in the synthesis of the solvent-free GNPs/PDMS composite and in manufacturing the electrode: a) a homogenous dispersion of GNPs in D_4 monomer was polymerized by TBPH at 110 °C for 1 h; b) at room temperature a multifunctional cyclosiloxane monomer that functions as cross-linker was added and mixed to obtain a homogenous composite; c) screen-printing the composite to electrodes with different shapes, which were thereafter cross-linked at 110 °C followed by deactivation of the initiator at elevated temperatures.

The potential of the newly developed electrode material is evaluated in stretch sensors and stack actuators. They were manufactured without using any solvent.

2. Results and Discussions

2.1. Synthesis and Characterization of Conductive Elastomer

The steps involved in GNPs/PDMS composites synthesis and electrode manufacturing are illustrated in **Figure 1**. GNP filler was used to achieve a conductive PDMS composite. This filler is known for its high thermal and electrical conductivity, alongside environmental stability.[46] Therefore, it may allow the formation of composites that will not deteriorate in time even under high voltages. Due to the low viscosity of D_4, the GNP filler can be dispersed by tip sonication without solvent. Uniform distribution of GNP in a composite is crucial for an electrode material, which should provide a homogenous electric field. The in situ anionic ring-opening polymerization (AROP) using tetra-butylphosphonium hydroxide (TBPH) transient initiator in the presence of GNPs enables the formation of more homogenous composites than those in which the filler is added to a preformed polymer.[46,47] Additionally, it leads to a better interaction between the filler and the polymer matrix, improving the stability of the composite. The thermodynamically controlled AROP of D_4 leads to an equilibrium of linear and cyclic products.[48,49] After 1 h polymerization at 110 °C, the mixture was cooled to room temperature, and the second monomer that functions as a cross-linker was added (Figure 1b). The cross-linker was prepared according to literature using a hydrosilylation reaction mediated by Karstedt's catalyst.[49]

The composite was then processed into thin films by screen-printing and cross-linked at 110 °C. After cross-linking, the catalyst was deactivated by heating the composite to 150 °C (Figure 1c). The deactivation of the transient catalyst is much simpler than the non-transient one, where repetitive washing with a large amount of solvent is needed. Note that neither for the synthesis of the composite nor processing into thin films solvent was used.

ADVANCED
SCIENCE NEWS

www.advancedsciencenews.com

[M]acro-
molecular
Rapid Communications

www.mrc-journal.de

Table 1. Electrical properties of the synthesized composites.

Sample	GNP [wt%]	$R_{0\%}$ [a)] [Ω]	Sheet $R_{0\%}$ [b)] [Ω sq^{-1}]	Sheet $R_{30\%}$ [b)] [Ω sq^{-1}]	Sheet $R_{50\%}$ [Ω sq^{-1}]*	$\Delta R/R_{0\%}$ [c)] at 30%	$\Delta R/R_{0\%}$ [c)] at 50%	Vol. σ at 0% [d)] [S cm^{-1}]	Resistivity[e)] at 0% [Ω cm^{-1}]
GNP3	3	372	553	3551	5896	5.42	9.66	0.602	1.66
GNP4	4	132	196	842	1686	3.30	7.60	1.703	0.59
GNP5	5	34	50	227	–	3.54	–	6.660	0.15
GNP6	6	28	41	141	395	2.44	8.63	8.175	0.12
Wacker	NN	1863	2754	5682	8433	1.06	2.06	0.048	20.66
CB	-	10 975	16 230	23 957	31 794	0.48	0.96	0.062	16.23

a) Resistance measured using a 4-point probe. b) Sheet resistance calculated from the resistance multiplied by the correction factor based on the sheet dimensions. c) Change in sheet resistance calculated from the measured sheet resistance at the given strain by subtracting the sheet resistance at 0% strain and dividing by the sheet resistance at 0% strain. d) Volume conductivity was calculated from the inverse of the sheet resistance multiplied by sample thickness. e) Resistivity calculated from inverse conductivity.

Firstly, we optimized the filler content to achieve the highest possible conductivity by gradually increasing its content from 3 to a maximum of 6 wt% (**Table 1**). The formed composites were named GNPx, where *x* represents the wt% of GNP in the PDMS matrix. For all these materials, the amounts of initiator and cross-linker were kept constant to 1.8 and 0.82 mol%, respectively. While the conductivity increased with the conductive filler content, we were limited to a maximum of 6 wt% of GNP. Above this concentration, the D_4 was practically absorbed on the GNP surface, rendering tip sonication impossible.

Stripes of composites GNPx on a PDMS film were made by screen-printing. The literature recommends at least two layers of screen-printed electrodes for actuator applications.[32,45] Therefore, the composites were three times screen printed on a PDMS film. After each printing step, the electrode was cross-linked and then the next layer was screen-printed. Thus, the electrodes are expected to exhibit a more homogenous electric field, a reversible response in an actuator, and a longer lifetime. The resistance of the composites decreased due to the triple printed layer's increased electrode thickness and homogeneity (Figures S1 and S2, Supporting Information). For instance, the resistance of GNP6 dropped from roughly 3.3 kΩ to 71 Ω from the first to the second layer and 28 Ω for the third layer.

The electrical properties of GNPx are compared to a commercial electrode by Wacker and carbon black powder brushed on a silicone film (Table 1). As can be seen in insert **Figure 2**a, increasing GNPs content leads to reducing resistance. All composites have a starting resistance value in the range of 28–372 Ω, which is significantly lower than that of Wacker electrode (1863 Ω) and carbon black powder brushed on a silicone film (11 kΩ). The percolation threshold is well below 3 wt% GNP as the conductivity already reaches 0.602 S cm^{-1} (10^{12} times higher than PDMS). Between 3 and 5 wt% the change in conductivity is still in the same order of magnitude, indicating that additional conductive paths are still formed. However, the change between 6.660 S cm^{-1} for GNP5 and 8.175 S cm^{-1} GNP6 is already small, appearing to get close to the typical S-shaped maximum curve conductivity of the composite.

The resistance was also measured at different uniaxial strain levels. A significant difference in the resistance change with strain for GNPx can be observed. The conductive network breaks down significantly faster for GNP3 than for GNP6. This is true not only for the absolute resistance value but also for the relative resistance change. However, even composite GPN3, with the lowest filler content, exhibited surprisingly high conductivity of 0.6 S cm^{-1} at 0% strain, but it shows a substantial reduction of conductivity upon straining. This conductivity drop is undesirable for an electrode, which should be conductive at large strains, but may be attractive for stretchable conductive or piezoresistive sensors.[50–53] Samples GNP4-6 showed lower starting resistance and a slower increase in resistance with strain. It appears that already with 4 wt% GNP, the conductive network is, to a larger part, retained at higher strains. The composites with 5 and 6 wt% GNP followed a similar trend for resistance change with strain as GNP4. Still, the starting sheet resistance decreased significantly from 196 Ω sq^{-1} for GPN4 to 50 Ω sq^{-1} for GPN5 and reached a minimum value of 41 Ω sq^{-1} for GNP6, respectively (Table 1). Composite GNP6 also showed a rather low sheet resistance even when strained by 80% (below 1 kΩ sq^{-1}), which increased to 6 kΩ sq^{-1} at 180% strain (Figure S3, Supporting Information). Its volume conductivity decreases moderately and its resistivity increases with strain (Table 1, Figure 2b).

The most conductive composite GNP6 showed a relatively small change in $\Delta R/R_0$ values for strains up to 60%, but increased at higher strain levels (Figure 2c). Although it is common to present the change in resistance $\Delta R/R_0$ with strain, this can be misleading, as only the relative change of resistance is observed. For actuators applications, the relative change in resistance often plays a minor role. More important is the absolute change in resistance, which will affect the actuator's speed of charging and discharging. The charging rate is given by the time constant (τ):
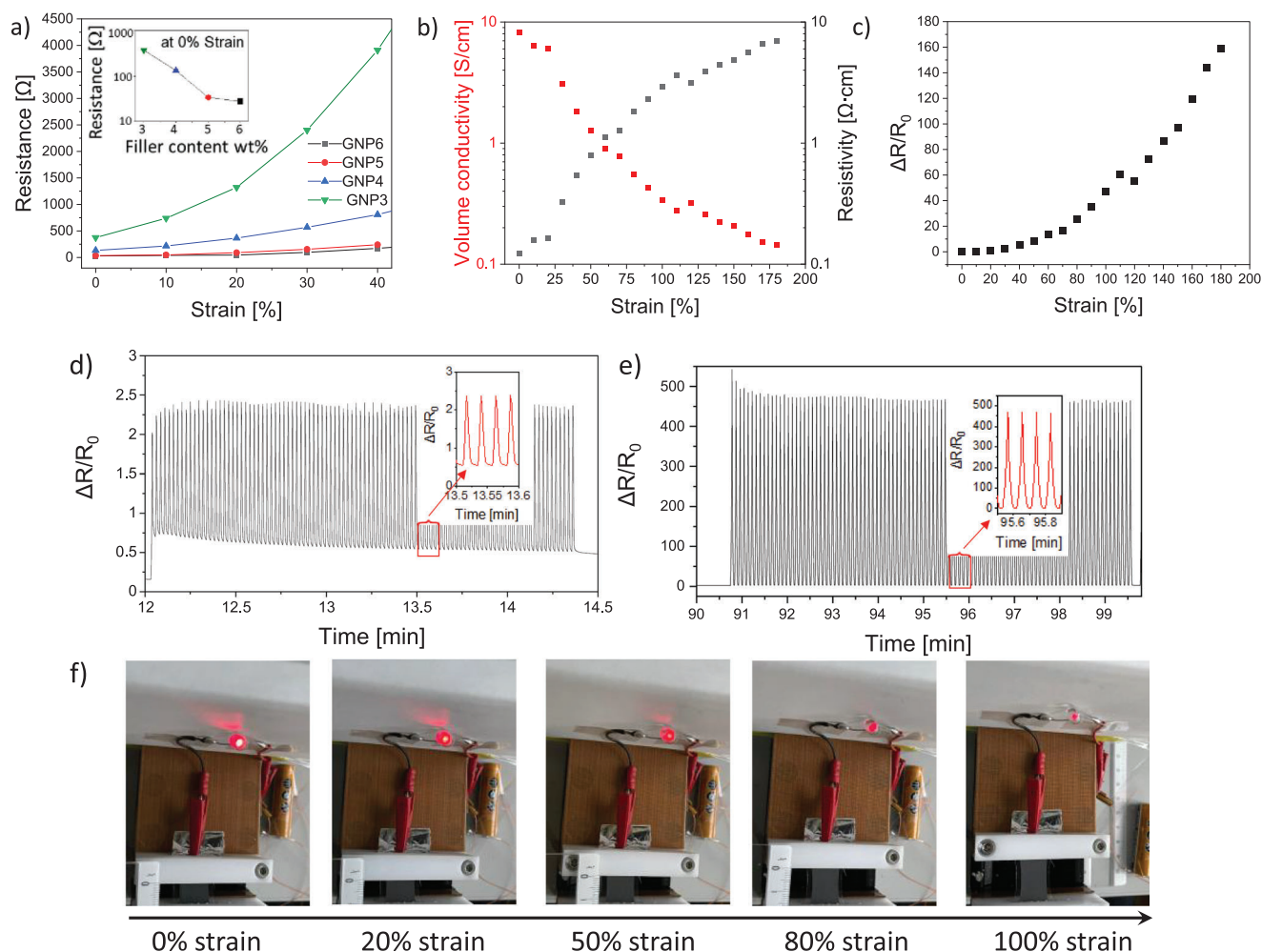
$$\tau = R \times C \qquad (1)$$

where C represents the capacitance and R resistance.

The resistance of GNP6 is low enough to fully charge typical DET devices with several hundred pF in under 100 ns even at higher strains and not to limit the maximum frequency required for some DET applications of up to 100 Hz.

Thus, the electrical conductivity and stretchability results show that the prepared electrode material GNP6 has good conductivity and is highly stretchable with sheet resistance below 7 kΩ sq^{-1} at 180% strain. Consequently, GNP6 should achieve high cycling speeds at all strain levels and is well suited for actuator and sensor applications. In the following, only GNP6 is further investigated.

**ADVANCED
SCIENCE NEWS**
www.advancedsciencenews.com

{M}acro-
molecular
Rapid Communications
www.mrc-journal.de

Figure 2. Resistance of GNPx composites with different GNP wt% loadings at varying strains and insert a) resistance of GNPx at 0% strain and electrical properties of composite GNP6: b) volume conductivity/resistivity change in c) $\Delta R/R_0$ for uniaxial strains up to 180%. Change in $\Delta R/R_0$ over 100 cycles for GNP6 screen-printed three times on a PDMS substrate and stretched from d) 0 to 30% at 0.83 Hz and from e) 0 to 130% at 0.19 Hz. Impact of stretching on a light-emitting diode operated by a 1.5 V battery and using GNP6 electrode at different strain levels: f) 0%, 20%, 50%, 80%, and 100% strain. Even at 100% strain, the electrode is still conductive, as seen by the light-emitting diode.
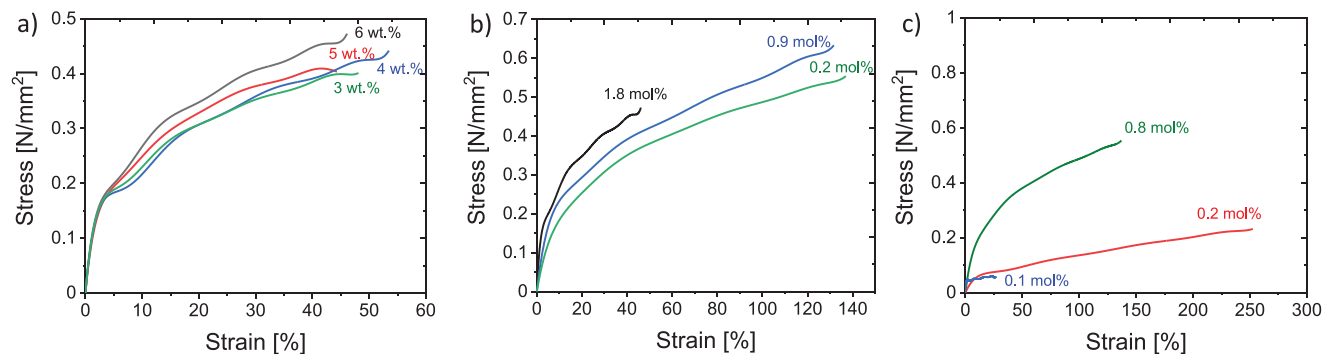
Another important aspect is the stability of the electrode during cycling at different strains and frequencies. GNP6 applied on a PDMS film was strained at different strain levels up to 150% with an increment of 10% at frequencies from 0.17 to 2.5 Hz for 100 cycles at a rate of 5 mm s^{-1}. In total, this resulted in 1500 cycles. A closer look at $\Delta R/R_0$ values at strains from 0% to 30% and 0% to 130% over 100 cycles at 0.83 and 0.19 Hz, respectively, showed a relatively reversible behavior (Figure 2d,e). A small hysteresis was observed within the first few cycles for $\Delta R/R_0$ at each defined strain, which stabilized fast. Thus, the electrode material showed similar behavior and high stability over all tested strains up to 150%.

To further illustrate the good conductivity at different strain levels, GNP6 was used to operate a LED by a standard 1.5 V AA battery. Even when the electrode was uniaxially strained to 100%, the LED emitted light (Figure 2f, Movies S1 and S2, Supporting Information).

Standard characterization of stretchable electrodes includes the change in conductivity under uniaxial strain. However, trans-

ducers are often strained equibiaxially. Composite GNP6 showed a similar trend as uniaxial strain when equibiaxially strained (Figure S3, Supporting Information). The electrode showed a change in resistance from 30 Ω at 0% strain to 250 Ω at 40% biaxial strain, which is attractive. An equibiaxial strain of 40%, representing a 96% areal expansion, would be sufficient for many DEA applications.

For many applications, the mechanical properties of the electrodes are not crucial, as they do not influence device performance. However, applications in sensors and actuators need to have a compliant electrode material. Therefore, we prepared freestanding electrodes with each composite by screen-printing them directly on a Teflon substrate. The electrodes could be easily detached as stripes from the Teflon after cross-linking. After stamping them into dog-bone-shaped samples, we investigated their properties by tensile testing (**Figure 3**, see Figure S4, Supporting Information for individual stress–strain curves). The strain at break, Young's modulus, and the maximum force at break are given in **Table 2**. The strain at break decreased from 90%

**ADVANCED
SCIENCE NEWS**

www.advancedsciencenews.com

[M] acro-
molecular
Rapid Communications

www.mrc-journal.de

Figure 3. Averaged stress-strain curves of: a) GNPx; b) GNP6 prepared using different amounts of TBPH initiator; and of c) GNP6 prepared using different amounts of cross-linker.

Table 2. Amount of GNP, cross-linker (CL), TBAH added to 10 mL D_4 monomer and mechanical properties (maximum strain s_{max}, maximum stress σ_{max}, elastic modulus at different strain levels $Y_{x\%}$) of the screen-printed composites as well as their thickness d.

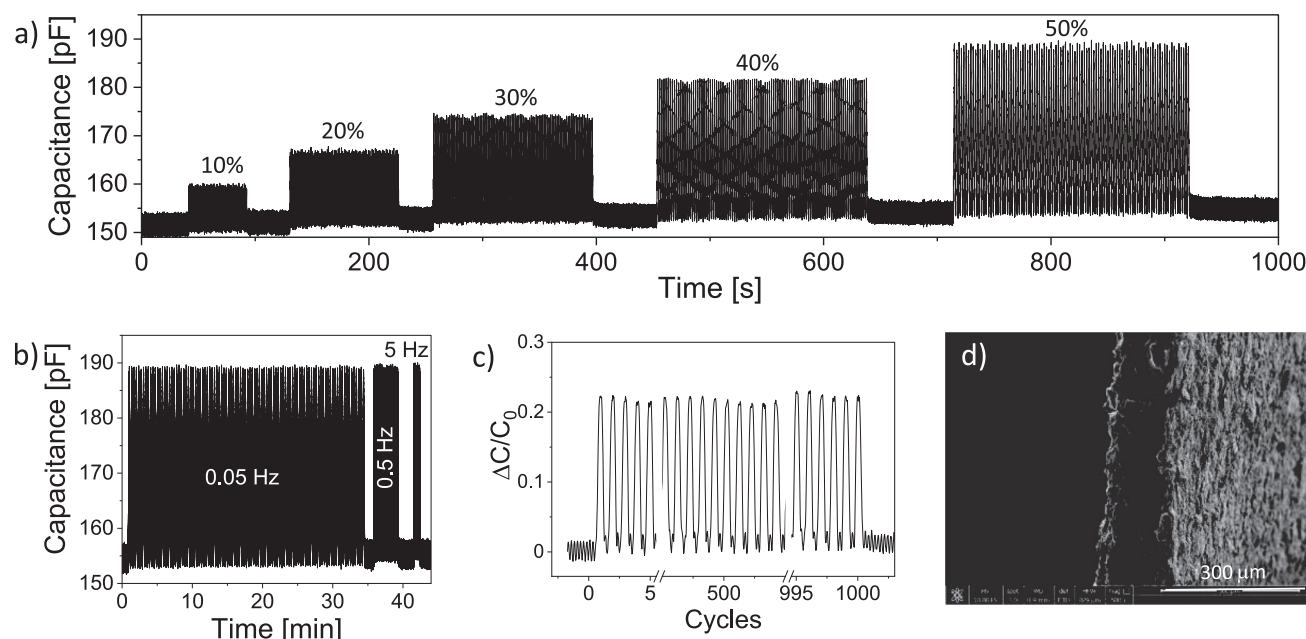| Entry	GNP [wt%]	CL		TBPH		s_{max} [%]	σ_{max} [N mm^{-2}]	$Y_{10\%}$ [kPa]	$Y_{20\%}$ [kPa]	d [µm]
		[µL]	[mol%]	[µL]	[mol%]					
1	6	200	0.82	400	1.80	74	0.534	1888	1303	33
2	5	200	0.82	400	1.80	52	0.405	1796	1217	40
3	4	200	0.82	400	1.80	65	0.446	1270	1027	30
4	3	200	0.82	400	1.80	90	0.477	1448	1045	32
5	6	200	0.82	200	0.90	158	0.685	1425	1076	30
6	6	200	0.82	50	0.22	185	0.612	1324	1042	55
7	6	50	0.20	50	0.22	305	0.235	167	146	50
8	6	25	0.10	50	0.22	27	0.062	116	87	56
9	-	50	0.20	50	0.22	741	0.225	71	64	123

to 52% with increasing GNP content from 3 to 5 wt%, respectively, but increased to 75% with increasing the GNP content to 6 wt%. Composite GNP6 has the highest Young's modulus and reached $Y_{10\%} = 1.88$ MPa. The elastic modulus of the composites was 4.09 times higher than the PDMS matrix that was prepared using the same amount of initiator and cross-linker without filler ($Y_{10\%} = 461$ kPa), showing the strong reinforcing effect GNPs have on the matrix.

PDMS chain length strongly impacts the mechanical properties of elastomers, e.g., shorter polymer chains result in a stiffer material compared to longer ones. The amount of initiator affects the PDMS chain length and thus can be used to optimize the mechanical properties of the final composite. Therefore, we first investigated how the amount of initiator affects the molar mass of the formed polymer. The viscosity and molar mass of the polymer increased with decreasing the amount of TBPH initiator from 1.8 to 0.9, and 0.22 mol%. A further reduction of TBPH was not possible because the GNP dispersion in D_4 did not polymerize. Therefore, for further experiments, the amount of TBPH was set to 0.2 mol%, and the cross-linker was optimized. The polymerization was conducted at 110 °C for 1 h to reach the thermodynamic equilibrium. The composite viscosity after the synthesis was 1720 Pa s at a shear rate of 0.01 s^{-1} and was found to be ideal for solvent-free processing by screen-printing (Figure S5, Supporting Information). This viscosity was sufficiently high

to allow printing without smearing the electrode after screen removal and sufficiently low to enable solvent-free screen-printing. The composite can be stored for a few days in the refrigerator before use. The cross-linker should be added to the composite just before processing.

Besides the chain length of PDMS, another way to tune the mechanical properties of the composite is the amount of cross-linker. Decreasing the amount of multifunctional monomer that functions as cross-linker allowed the formation of softer materials with high strain at break (Table 2, Entry 6–8). For comparison, the PDMS with and without filler is depicted. The impact of initiator and cross-linker amounts used on the mechanical properties of the formed composites can be observed in Figure 3 and Table 2. The lowest average strain at break of 74% was observed for the composite prepared with the highest amount of filler, initiator, and cross-linker (Table 2, Entry 1), while the highest strain at break of 305% was measured for the composite for which both the amount of initiator and cross-linker were significantly reduced (Table 2, Entry 7). The highest tensile strength of 0.685 N mm^{-2} was observed for composite Entry 5, while the lowest of 0.062 N mm^{-2} was recorded for composite Entry 8. The lowest Young's modulus was measured in Entry 8 with an average of $Y_{10\%} = 116$ kPa and $Y_{20\%} = 87$ kPa, respectively. In contrast, the highest average Young's modulus was observed in Entry 1 with $Y_{10\%} = 1888$ kPa and $Y_{20\%} = 1303$ kPa.

**ADVANCED
SCIENCE NEWS**

www.advancedsciencenews.com

{M}acro-
molecular
Rapid Communications

www.mrc-journal.de

Figure 4. Capacitance sensor based on a commercial silicone and composite GNP6 electrode: a) change in capacitance over 100 cycles at different strain levels using a 10% step increase in strain up to a maximum of 50% strain. b) Change in capacitance over 100 cycles at 50% strain and different frequencies of 0.05, 0.5, and 5 Hz. c) Enlargement of the relative change in capacitance of a sensor strain at 5 Hz for a total of 1000 cycles: first cycles 0–5, cycles 495–505, and cycles 995–1000. d) SEM micrographs of the cut capacitor after being stretched 500 000 times at 50% strain. No delamination can be observed.

From all synthesized composites, composite Entry 7 was best for DET applications. It shows a conductivity of 8.2 S cm^{-1}, a very low Young's modulus $Y_{10\%} = 167$ kPa and $Y_{20\%} = 146$ kPa, a relatively high average strain at break of 305%, and last but not least, it can be screen-printed solvent-free.

Compliant electrode materials are desirable to prevent device stiffening, which degrades sensor and actuator performance. However, there are many applications where a low Young's modulus is less critical as in hydraulically amplified electrostatic actuators, flexible electronics, and energy generators. However, for all these applications, it is highly desirable to have a solvent-free conductive formulation that can be easily printed, does not interfere with the substrate on which it is printed, and does not peel off the substrate. The newly developed electrode material was successfully printed on different substrates, including PDMS, PET, polypropylene (PP), and polyethylene (PE). The chemistry used for cross-linking allows for strong adhesion of the electrode material to different substrates, which was verified by applying a piece of 3M Scotch tape to the conductive surface. The test showed no detachment of the electrode. Additionally, the excellent adhesion of the electrode to PET was demonstrated with a ribbon actuator tested at different frequencies from 0.1 to 10 Hz (Movie S3, Supporting Information).[54]

To sum up, the optimized GNP6 material showed a high starting conductivity of 8.2 S cm^{-1}, relatively low change in resistivity for up to 80% uniaxial strains, a low elastic modulus of 167 kPa, and a large strain at break of 305%. Although the conductivity of GNP6 is significantly lower compared to stretchable elastomers consisting of Ag fillers embedded in an elastic matrix, it is sufficiently high for DET applications and shows no hysteresis under repetitive stretching.[55,56] Additionally, solvent-free manufactur-

ing allows screen printing on virtually any substrate, while the chemistry used facilitates an excellent adhesion to the substrate, preventing delamination.

2.2. Capacitive Sensors

The functionality of the newly developed electrode material was tested in stretchable capacitive sensors using a commercial silicone as a dielectric. These sensors require excellent stability during stretching at high strains and high frequencies, which can be affected by the electrode performance. Hence, the capacitance measurement at different strains and frequencies gives insights into the reliability and stability of the electrode material. The capacitance (C) is given by $C = \epsilon_0 \epsilon'' A/d$, where ϵ_0 is the vacuum permittivity, ϵ'' is the relative permittivity, A is the area, and d is the thickness. It increases with the electrode area and thinning the dielectric layer. The change in capacitance was recorded at different strain levels using a 10% step increase in strain, up to a maximum of 50% strain. For each strain level, 100 cycles were recorded at a strain speed of 5 mm s^{-1} (**Figure 4**). These tests show stable and reversible capacitance changes. The capacitance at 0% strain was 152 ± 2 pF. It increased to 160 pF at 10% strain and reached the highest tested value of 190 pF at 50% strain.

Additionally, the sensor was tested for 100 cycles at 10% strain and 0.25, 2.5, and 25 Hz as well as at 50% strain and 0.05, 0.5, and 5 Hz (Figure 4b). The change in capacitance at 50% strain was the same at frequencies of 0.05, 0.5, and 5 Hz, suggesting that our electrode is sufficiently conductive to allow reliable sensor operation at frequencies up to 5 Hz. The capacitance stayed constant at a value of 190 pF at 50% strain and around 155 pF

**ADVANCED
SCIENCE NEWS**

www.advancedsciencenews.com

Macro-
molecular
Rapid Communications

www.mrc-journal.de

at 0% strain, respectively. Furthermore, a sensor tested at 50% strain and 5 Hz over thousand cycles shows no hysteresis, which further confirms the excellent properties of our electrode (Figure 4c).

The sensor was then strained from 0 to 50% strain 500 000 times at 5 Hz and was intentionally ruptured by increasing the strain. Scanning electron microscopy (SEM) images of the resultant fracture surface (Figure 4d and Figure S6, Supporting Information) showed no electrode delamination from the dielectric film, which confirms strong adhesion and compliance between electrode and dielectric.

2.3. Single-Layer Actuators

Screen-printing without solvent leads to 20–50 μm thick electrodes. Such thick electrodes may affect the actuation as the entire device stiffens. Thinner electrodes can be produced, but a different screen or coating technique has to be used. To understand the impact a particular electrode material has on actuation, single-layer actuators were made by spray coating a solution of GNP6: ethylacetate through a shadow mask on both surfaces of the dielectric film. The thickness was controlled via typical spray coating parameters such as dilution, time of spraying, or N_2 pressure. When a solution of GNP6: ethyl acetate of 1:2 was used, the sprayed electrodes were rather thick. However, further reducing the GNP6: ethyl acetate to 1:10 weight allowed the formation of thinner and more homogenous layers. The results were compared with membrane actuators made with carbon black powder electrodes and showed that our electrode material does not stiffen the actuator (Figure S7, Supporting Information). Even the actuators with an electrode thickness of up to 55 μm showed a similar performance to carbon black brushed on a 150 μm thick dielectric film. The good performance of the actuator is due to the low Young's modulus of 167 kPa for the optimized electrode material. This allows the construction of actuators with soft electrodes. They are an order of magnitude softer than composite electrodes prepared using commercial polymer matrices with Young's modulus typically above 1 MPa.[57] Devices constructed with such an electrode material and an electrode to a dielectric ratio of 1:4 showed significant stiffening reflected in a 45% lower actuation than actuators with dry carbon powder as electrodes.

The stability of our electrode material was evaluated with an actuator whose dielectric was Elastosil 100 μm thick prestrained by 7.5% on which side electrodes (44 μm thick) with a diameter of 7 mm were sprayed. It was subjected to 5600 V for 10 000 cycles at 1 Hz. While the lateral actuation is not high since the silicone film has a permittivity of 3 and an elastic modulus of about 1.2 MPa, it shows almost no hysteresis confirming the high stability of GNP6 at high repeated voltages (Figure S7e, Supporting Information).[58]
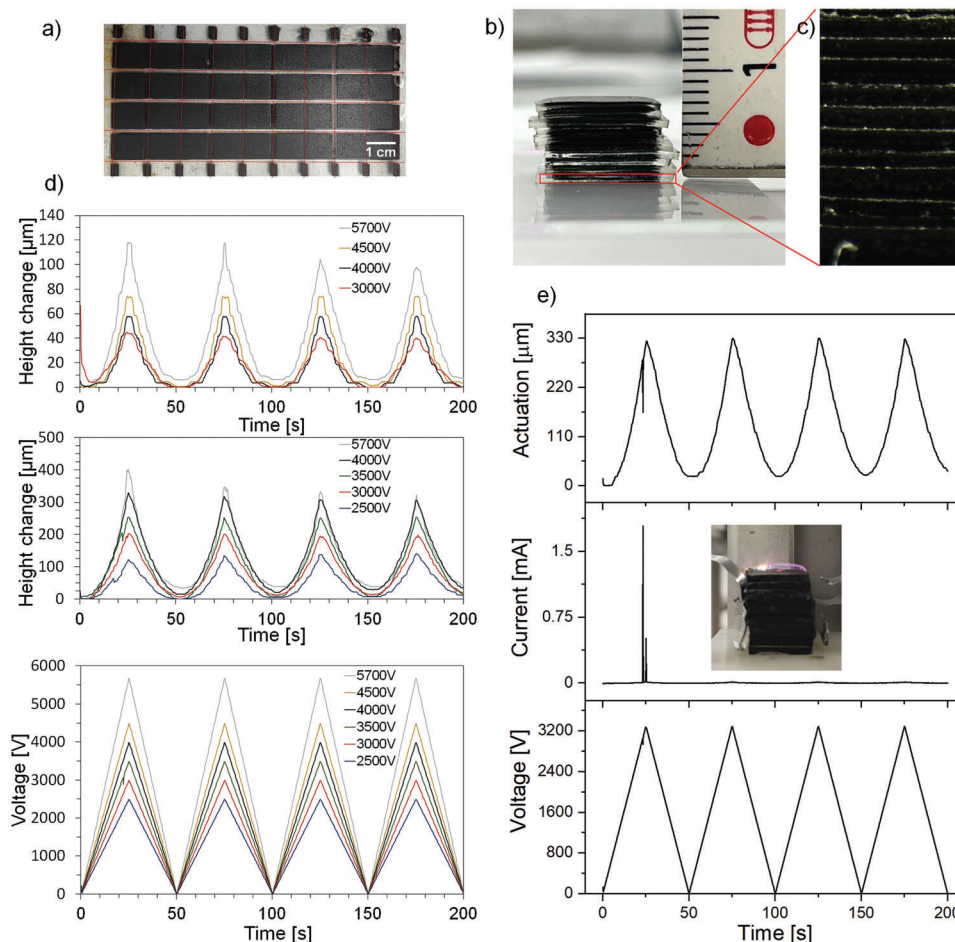
2.4. Stack Actuators

Stack actuators with a dielectric silicone prepared by the solvent-free process described above were constructed using the optimized GNP6 electrode. The stacks were made by doctor blading the dielectric layer and cross-linking at 110 °C, followed by screen-printing the electrode material on the dielectric and cross-linking at 110 °C. The electrode material was screen-printed three times to ensure a homogenous and complete coverage of the dielectric by the electrode. Following these steps, stacks consisting of five alternating layers of dielectric and electrode were manufactured (**Figure 5**). Note that the entire dielectric and electrode composite synthesis process to stack actuator manufacturing was solvent-free. This is the first stack actuator manufactured by a green, economical, and environmentally friendly process to the best of our knowledge.

The printed layers were cut into 1×1 cm^2 pieces, which resulted in stack actuators consisting of five active layers, with a dielectric layer thickness of 100 μm and an electrode thickness of 30 μm. Thereafter, ten of the five layers actuators were manually placed on top of each other to produce a stack actuator consisting of 50 active layers. The electrical connection of the active layers in the stack was achieved manually with the help of a cotton swab. Two different materials were used: carbon black powder and GNP6. As described later, the kind of material used to connect the active layers affected the stack lifetime. The connection of the stack to the high voltage source was made with two aluminum stripes that touch the stack on the conductive sides. The voltage was increased within 25 s from 0 V to a predefined voltage and then decreased to 0 again within 25 s, while a laser measured the change in the stack thickness. The actuator was tested at defined voltages for four cycles up to a maximum voltage of 5700 V provided by the voltage source. The expected increase in the actuation strain was observed with increasing the voltage, and the actuation was reversible. A maximum actuation of 120 μm was measured at 5700 V and 20 MHz, which represents a thickness change of 1.8% (Movie S4, Supporting Information). However, a breakdown was observed at this voltage, which is reflected by a slight decrease in actuation in the cyclic test. Despite this, the actuator still functions because it can self-repair. Contrary, stack actuators with carbon black powder connecting the layers showed no self-repairing and the breakdown event caused the burning of large stack areas.

The compatibility of the newly developed electrode material was demonstrated using another dielectric material, a commercial silicone from Wacker, which was solvent-free manufactured into thin films with a thickness of 200 μm. Also here, a voltage increase led to a fast height change of the stack actuator. For instance, at 2500 V the stack height changed by 125 μm, at 3000 V by 200 μm, at 3500 V by 250 μm, and at 4000 V by 325 μm, respectively. When the voltage was increased to 5700 V, the actuator contracted by roughly 425 μm (3.5%), but the actuation declined to about 325 μm after already four cycles. Nevertheless, actuation at voltages up to 4000 V was reversible and showed no hysteresis between cycles. At 5700 V, a decrease in actuation was observed due to a breakdown, which irreversibly deactivated parts of the actuator and led to a lower actuation. The breakdown, however, did not lead to a complete failure of the actuator. During the cyclic testing of the stacks, multiple local breakdowns (observed by spikes in current flow) were observed, which did not fatally damage the stacks. The insert in Figure 5e shows the image of a discharge event, which occurred through the air (Movie S4, Supporting Information). Despite this event, which resulted in a voltage drop, an increase in current to 2.5 mA, and an immediate reduction in actuation, the actuator was not damaged.

**ADVANCED
SCIENCE NEWS**

www.advancedsciencenews.com

acro-
olecular
Rapid Communications

www.mrc-journal.de

Figure 5. a) Representative images of a 9 × 4 printed five layers stack; b) 3D stack actuator composed of 50 active layers with a total active area of 50 × 1 cm^2; c) optical image of the layers in the stack; d) actuation of a stack consisting of a self-made (top) and d) commercial silicone elastomer (middle) as dielectric and the corresponding applied voltage (bottom). A self-repairing event in a stack actuator operated at 3200 V. e) A drop in actuation and an increase in the leakage current can be observed, followed by self-repairing with a full recovery of initial actuation. The insert is the image of the discharge event.

It showed a reversible actuation at 3300 V. Hence, the electrode material can handle high voltages with sudden discharges and breakdowns without damaging large areas. Several groups have reported self-clearing of actuators for different carbon-based electrode materials.[19,21,25,32] However, to the best of our knowledge, self-clearing has not been shown in stacked DEA. In addition to the benefit of self-repairing, the entire process described here is scalable and allows the formation of actuators with similar performance. A total of nine 50 layers DEA stacks were prepared and all showed a similar response (Figures S8–S10, Supporting Information).

Ten layers stack actuator with our PDMS elastomer as dielectric and screen-printed GNP6 electrode with an active area of each layer of 1 × 1 cm operated at 1 Hz for 90 cycles at 4000 V. Same hysteresis can be observed at the beginning, but then the actuation stabilized (Figure S11, Movie S5, Supporting Information).

The functionality of the newly developed electrode material was also proven in rolled actuators manufactured as described by Kovacs and co-workers (Movie S6, Supporting Information) and further confirms the applicability of our electrode material.[59,60]

These experiments confirm that our electrode material is also suitable for application at rather high voltages. This work will advance the field of dielectric elastomer actuators, where a material that combines good electrical and mechanical properties with stability under high voltages and easy synthesis and manufacturing was missing. Additionally, the self-repairing ability of actuators by the electrode material will significantly increase actuator's lifetime and reliability.[61,62]

3. Conclusion

We developed a solvent-free synthesis of a conductive electrode based on GNP in a PDMS matrix using anionic polymerization of cyclosiloxane monomers. The cross-linked material is conductive, flexible, stretchable, compliant to the dielectric material, and can be processed solvent-free by screen-printing. The electrode with a GNP content of 6 wt% has a starting sheet resistance of 40 Ω sq^{-1} and a change in resistivity of up to 180% lateral strain that does not affect DET performance. Additionally, the mechanical properties of the electrode can be easily tuned by the amount

of initiator and cross-linker. The softest electrode material has a very low Young's modulus of 167 kPa, and a strain at break of 305%. Capacitive stretchable sensors constructed with this electrode showed no degradation after being stretched 500 000 times at 50% strain and 2.5 Hz. Additionally, single-layer actuators can be produced by screen-printing or spraying a solution of the electrode in ethyl acetate with an airbrush. The actuators show no degradation at high voltages. Furthermore, 50-layer stack actuators were easily produced using a layer-by-layer technique, in which the electrode is screen-printed on a dielectric film prepared by doctor blading. The formed stacks give a displacement of 3.5% at 5700 V (30 V μm^{-1}). Moreover, the electrode material exhibited self-clearing capabilities improving the fault tolerance of the stack. The potential of newly developed material was demonstrated in capacitive sensors and actuators, however, we foresee that they could also be used for other applications such as generators, hydraulically amplified electrostatic and ribbon actuators, and printable electronics. Our simple synthesis can be easily extended to a plethora of other conductive, semiconductive, and insulator fillers to produce a wide range of different solvent-free composites with tailor-made electromechanical properties.

4. Experimental Section

Experimental Materials: Octamethylcyclotetrasiloxane (D_4), heptamethylcyclotetrasiloxane (D_4H), platinum-divinyltetramethyldisiloxane complex (Karstedt's catalyst) as well as trivinylmethylsilane were purchased from ABCR. Tetrabutylphosphonium hydroxide (TBPH) solution 40 wt% in H_2O, toluene, and heptane were purchased from Sigma-Aldrich. GNP grade M-25, thickness 6–8 nm, diameter 25 μm, and a surface area of 120–150 $m^2\ g^{-1}$ were purchased from xG Sciences Inc., USA. SLM LE 2854A and SLM LE 2854B were purchased from Wacker. All materials were reagent grade and used as received without further purification. The cross-linker was prepared as previously reported.[49]

Composites of GNP in PDMS: The filler material GNP (varying weight percentages, refer to Table 1) was dispersed in D_4 (10 mL) by tip sonication for 60 min (2 s pulse, 2 s pause, at 40% power), while being cooled with a water bath. Subsequently, the mixture was heated to 110 °C while mechanically stirred (300 rpm) under a constant argon stream. After 5 min at 110 °C varying mole percentages of TBPH were added (Table 2). The reaction was heated for 1 h at 110 °C under continuous stirring. After cooling to room temperature, the cross-linker (Table 2) was added to the composite, which was then mechanically mixed for 5 min (300 rpm) and sonicated for another 5 min. The mixture was screen-printed onto a PDMS substrate and cross-linked at 110 °C for 20 min. The screen-printing and cross-linking process was repeated three times, after which the catalyst was decomposed by heating to 150 °C for 30 min.

Synthesis of PDMS with Active Chain Ends from D_4: D_4 (30 mL) was heated to 110 °C under constant mechanical stirring (300 rpm) in a three-neck flask. After 5 min at 110 °C TBPH (0.15 mL) was added. The mixture was reacted for 1 h under a constant argon stream to allow water to gas out. After 1 h, the mixture was cooled to room temperature.

PDMS Dielectric: To a PDMS with active chain ends (7 g) prepared by reacting D_4 (10 mL), TBPH solution (0.05 mL) for 1 h at 110 °C the multifunctional monomer cross-linker (200 μL) was added and stirred at room temperature to give a homogenous mixture. The mixture was cast on a glass substrate by doctor blading (blade thickness of 100 μm) at a speed of 1 mm s^{-1} and then cross-linked for 20 min at 110 °C. Finally, the catalyst was decomposed at 150 °C for 30 min.

The dielectric silicone from Wacker was prepared by mixing silicones SLM LE 2854A and SLM LE 2854B by a 1:1 by weight ratio. The mixture was cast on a Teflon substrate by doctor blading (blade thickness of 200 μm) at a speed of 1 mm s^{-1}. The substrate was cross-linked for 20 min at 110 °C.

Screen-Printing of the Electrode and Doctor Blading of DE Layers for Stacked Actuators: To a GNP composite in PDMS synthesized starting from D_4 (30 mL), GNP (1.72 g), TBPH solution (0.2 mL) for 1 h at 110 °C, the cross-linker was added (200 μL) at room temperature and stirred to obtain a homogenous mixture. This mixture was screen-printed using a screen from Serilith AG (mesh 61–64 W, 105 $cm^3\ m^{-2}$, 23 × 36 cm) on top of a PDMS dielectric film. The electrode was cross-linked at 110 °C for 20 min. The screen-printing of the electrode was repeated three times, followed by decomposition of the catalyst at 150 °C (Figure 1c).

Stack Actuators: Stack actuators were manufactured using a layer-by-layer coating. First, the dielectric was made by blading, and second, the electrode was made by screen-printing. Thereafter, the blade thickness was increased by the thickness of the previous layers plus 100 μm for the new dielectric layer. This process was repeated several times to achieve five active layers.

Stacking of the Five-Layered Actuators: The stack layers were cut into 1.1 × 1.1 cm pieces (1 × 1 cm active electrode). Ten of them were stacked on top of each other to give a 50 layer stack actuator. Finally, the electrodes within the stack were connected with the conductive composite brushed on the two opposite sides using a cotton swab. The two electrodes were connected to a FUG HCL-35-12500 high voltage source with aluminum foil to charge the stack. The voltage was gradually increased to 5700 V at a frequency of 25 mHz. A laser placed above the stack was used to sense the change in actuator height during actuation.

Single-Layer Actuators: The electrode material was diluted with ethyl acetate at a weight ratio of 1:2 and 1:10 (electrode: EtOAc) and stirred for 30 min to obtain a homogenous solution. An airbrush (Infinity by Harder&Steenbeck) with 2 bar N_2 pressure was used to spray the electrode (ϕ = 7 mm) through a shadow mask onto the dielectric material pre-strained by 7.5% and fixed into a rigid Teflon frame. A round shadow mask with a rectangular supply line for the voltage was prepared by laser-cutting a 140 μm thick poly(ethylene terephthalate) PET foil with a TruMark Station 5000 from Trumpf. After applying the electrode material, the actuators were cured and post-cured by heating at 110 and 150 °C in the oven, respectively. Reference actuators with carbon black powder electrodes with a diameter of 7 mm applied manually by a brush were also made.

A FUG HCL-35-12 5700 high voltage source served as a power supply for actuator tests at ambient temperature and humidity. A 100 V step every 2 s up to breakdown, or the maximum voltage of 5700 V delivered by the voltage source, was applied. The actuation strain was measured optically as the extension of the diameter of the electrode area via a digital camera, using an edge detection tool of a Lab-View program to detect the boundary between the black electrode area and the transparent silicone film.

Capacitor Sensor: Capacitor sensors were prepared by screen-printing the electrode three times on a 150 μm thick PDMS layer on both sides. The capacitor sensor was 1.5 cm wide and 2 cm long. After fixing it into the stretching setup, the active sensor length was 1 cm. After multiple tests at varying frequencies, the sensor was stretched 50% with a speed of 50 mm s^{-1} and frequency of 5 Hz over 500 000 cycles without the sensor's failure.

Characterization Methods: Details about characterization methods can be found in the Supporting Information.

Thin-film preparation by Doctor Blading was performed using a doctor blade ZUA 2000 by Zehntner GmbH.

The electrode samples used for mechanical testing were prepared by screen-printing three layers of composite directly on a Teflon substrate, while those for electrical characterizations were dome by screen-printing three times on PDMS film. The PDMS films were prepared by doctor blading on a Teflon substrate. The thickness of the samples was determined using a Heidenhain MT25B digital read-out system.

Microscopic images were taken with an Olympus SZX16 integrated with a digital Nikon camera system.

Scanning electron microscopy images were obtained with a Nova NanoSEM 230 FEI.

Tensile measurements were performed with a Zwick Z010 tensile test machine with a 50 mm min^{-1} speed using dog-bone shaped samples of 18 mm length and 2 mm width. The stress–strain curves were averaged from 3 independent samples per material, and the reported values were

**ADVANCED
SCIENCE NEWS**

www.advancedsciencenews.com

**Macro-
molecular
Rapid Communications**

www.mrc-journal.de

averaged. The Young's moduli were determined from the linear fit slope of the stress–strain curves from $0 \leq 10\%$ or $0 \leq 20\%$ strain as indicated.

Rheology measurements were performed using a disposable plate/plate setup with a diameter of the plates of 20 mm and a distance of 1 mm. Oscillation rheology was conducted to follow the cross-linking process. The setup was a plate–plate system measured at 25 °C. An amplitude sweep from 0.001–100% deformation in oscillatory measurement at a frequency of 10 rad s^{-1} and 25 °C was used. The frequency sweep from 0.05–500 rad s^{-1} in the oscillatory measurement was done at 1% amplitude. The flow curve in rotational measurement was done from 0.05–500 1 s^{-1}.

Electromechanical Characterization: The uniaxial stretching four-point probe measurements were performed by lateral stretching of the screen-printed composite on a PDMS matrix. The samples with a width of 1.5 cm and a length of 2 cm were fixed into the setup by clamps on the two ends, leaving a distance of 1 cm between the connections. The power source for the direct current ($I = 4.5$ mA) was connected using aluminum foil/silver paste and crocodile clamps. Multimeter pins were applied at a distance of 1 cm on the top of the sample supported by a small bench to prevent stretching by pins. After measurement, the voltage pins and the bench support were disengaged from the electrode and the samples were strained further. The electrical resistance was calculated according to Ohms law. Based on the correction value for finite sample sizes, the sheet resistance (R_s) was calculated based on $R_s = C'' \times V/I$, where C'' is the correction factor based on the dimensions of the sample and the four-point probe, V is the voltage, and I is the current.[63] The correction factor thereby was $C' = 1.4788$. The volume conductivity (σ) was calculated according to $\sigma = 1/(R_s \times d_e)$, where d_e is the thickness of the electrode. The starting thickness is $d_0 = 30$ μm. The thickness d_e, decreases during stretching as the length l increases, and was calculated for each stretch level $d_x = (d_0 \times l_0)/l_x$, where d_0 is the starting thickness, l_0 is the starting length and l_x is the length at a specific strain and d_x the thickness at a specific strain. The resistivity is the reciprocal value of the conductivity. Lastly, the change in resistance ($\Delta R/R_0$) was calculated from $\Delta R/R_0 = (R_x - R_0)/R_0$, where R_x is the measured resistance at a specific strain level and R_0 is the resistance value of the unstrained electrode. The relationship between resistance, sheet resistance, conductivity, and change in resistance with stretch for GNP6 is given in Figure 2a–d.

The stretching speed and the strain were controlled via Zaber Console software and a python script. The cyclic behavior was tested with a two-point probe setup. The standard cyclic speed was 5 mm s^{-1}. A Keithly DMM6500 ½ digital multimeter controlled via Kickstart software was used.

The biaxial stretching was performed with an additional biaxial home-made stretching setup, as described by Rosset et al., connected to the lateral stretching machine, which ensured automatized stretching.[31] The connection to the multimeter and power source was analog to the four-point probe setup described above.

Supporting Information

Supporting Information is available from the Wiley Online Library or from the author.

Acknowledgements

Conflict of Interest

The authors declare no conflict of interest.

Data Availability Statement

The data that support the findings of this study are available in the supplementary material of this article and the raw data used to generate the figures can be found at http://doi.org/10.5281/zenodo.5902623.

Keywords

[1] J. C. Yang, J. Mun, S. E. Y. Kwon, S. Park, Z. Bao, S. Park, *Adv. Mater.* **2019**, *31*, 1904765.
[2] R. Pelrine, R. Kornbluh, G. Kofod, *Adv. Mater.* **2000**, *12*, 1223.
[3] D. Chen, Q. Pei, *Chem. Rev.* **2017**, *117*, 11239.
[4] R. Pelrine, R. Kornbluh, J. Joseph, R. Heydt, Q. Pei, S. Chiba, *Mater. Sci. Eng., C* **2000**, *11*, 89.
[5] D. M. Opris, *Adv. Mater.* **2018**, *30*, 1703678.
[6] J. E. Q. Quinsaat, F. A. Nüesch, H. Hofmann, D. M. Opris, *RSC Adv.* **2013**, *3*, 6964.
[7] J. E. Q. Quinsaat, T. De Wild, F. A. Nüesch, D. Damjanovic, R. Krämer, G. Schürch, D. Häfliger, F. Clemens, T. Sebastian, M. Dascalu, D. M. Opris, *Composites, Part B* **2020**, *198*, 108211.
[8] N. Matsuhisa, M. Kaltenbrunner, T. Yokota, H. Jinno, K. Kuribara, T. Sekitani, T. Someya, *Nat. Commun.* **2015**, *6*, 7461.
[9] O. A. Araromi, S. Rosset, H. R. Shea, *ACS Appl. Mater. Interfaces* **2015**, *7*, 18046.
[10] N. Matsuhisa, X. Chen, Z. Bao, T. Someya, *Chem. Soc. Rev.* **2019**, *48*, 2946.
[11] S. Huang, Y. Liu, Y. Zhao, Z. Ren, C. F. Guo, *Adv. Funct. Mater.* **2019**, *29*, 1805924.
[12] S. Rosset, C. De Saint-Aubin, A. Poulin, H. R. Shea, *Rev. Sci. Instrum.* **2017**, *88*, 105002.
[13] T. Gisby, *Smart Mater. Struct.* **2018**, *27*, 74002.
[14] Y. Bai, Y. Jiang, B. Chen, C. C. Foo, Y. Zhou, F. Xiang, J. Zhou, H. Wang, Z. Suo, *Appl. Phys. Lett.* **2014**, *104*, 062902.
[15] S. Rosset, H. R. Shea, *Appl. Phys. A* **2013**, *110*, 281.
[16] C. Gong, J. Liang, W. Hu, X. Niu, S. Ma, H. T. Hahn, Q. Pei, *Adv. Mater.* **2013**, *25*, 4186.
[17] D. Mccoul, W. Hu, M. Gao, V. Mehta, Q. Pei, *Adv. Electron. Mater.* **2016**, *2*, 201500407.
[18] R. Ma, S.-Y. Chou, Y. Xie, Q. Pei, *Chem. Soc. Rev.* **2019**, *48*, 1741.
[19] W. Yuan, L. B. Hu, Z. B. Yu, T. Lam, J. Biggs, S. M. Ha, D. J. Xi, B. Chen, M. K. Senesky, G. Grüner, Q. Pei, *Adv. Mater.* **2008**, *20*, 621.
[20] W. Hu, R. Wang, Y. Lu, Q. Pei, *J. Mater. Chem. C* **2014**, *2*, 1298.
[21] H. J. Sim, H. Kim, Y. Jang, G. M. Spinks, S. Gambhir, D. L. Officer, G. G. Wallace, S. J. Kim, *ACS Appl. Mater. Interfaces* **2019**, *11*, 46026.

**ADVANCED
SCIENCE NEWS**

www.advancedsciencenews.com

**[M] acro-
olecular
Rapid Communications**

www.mrc-journal.de

[22] I. Burda, C. Baechler, S. Gardin, A. Verma, G. P. Terrasi, G. Kovacs, *Sens. Actuators, A* **2018**, *279*, 712.

[23] C. Pan, Y. Ohm, J. Wang, M. J. Ford, K. Kumar, S. Kumar, C. Majidi, *ACS Appl. Mater. Interfaces* **2019**, *11*, 42561.

[24] J. Shao, L. Yu, A. L. Skov, A. E. Daugaard, *J. Mater. Chem. C* **2020**, *8*, 13389.

[25] Z. Peng, Y.e Shi, N. Chen, Y. Li, Q. Pei, *Adv. Funct. Mater.* **2021**, *31*, 2008321.

[26] X. Ji, A. El Haitami, F. Sorba, S. Rosset, G. T. M. Nguyen, C. Plesse, F. Vidal, H. R. Shea, S. Cantin, *Sens. Actuators, B* **2018**, *261*, 135.

[27] N. Kobayashi, H. Izumi, Y. Morimoto, *J. Occup. Health* **2017**, *59*, 394.

[28] R. R. Da Silva, M. Yang, S.-I.l Choi, M. Chi, M. Luo, C. Zhang, Z. -. Y. Li, P. H. C. Camargo, S. J. L. Ribeiro, Y. Xia, *ACS Nano* **2016**, *10*, 7892.

[29] Y. Wang, C. Zhu, R. Pfattner, H. Yan, L. Jin, S. Chen, F. Molina-Lopez, F. Lissel, J. Liu, N. I. Rabiah, Z. Chen, J. W. Chung, C. Linder, M. F. Toney, B. Murmann, Z. Bao, *Sci. Adv.* **2017**, *3*, e1602076.

[30] T. Lam, H. Tran, W. Yuan, Z. Yu, S. Ha, R. Kaner, Q. Pei, *Electroact. Polym. Actuators Devices* **2008**, *6927*, 69270O.

[31] S. Rosset, O. A. Ararom, S. Schlatter, H. R. Shea, *J. Vis. Exp.* **2016**, *108*, e53423.

[32] J. E. Q. Quinsaat, I. Burda, R. Krämer, D. Häfliger, F. A. Nüesch, M. Dascalu, D. M. Opris, *Sci. Rep.* **2019**, *9*, 13331.

[33] T. V. Neumann, M. D. Dickey, *Adv. Mater. Technol.* **2020**, *5*, 2000070.

[34] A. B. M. Tahidul Haque, R. Tutika, M. Gao, A. Martinez, J. Mills, J. Arul Clement, J. Gao, M. Tabrizi, M. Ravi Shankar, Q. Pei, M. D. Bartlett, *Multifunct. Mater.* **2020**, *3*, 044001.

[35] S. Park, K. Mondal, R. M. Treadway, V. Kumar, S. Ma, J. D. Holbery, M. D. Dickey, *ACS Appl. Mater. Interfaces* **2018**, *10*, 11261.

[36] Y. Wang, Q. Liu, J. Zhang, T. Hong, W. Sun, L. Tang, E. Arnold, Z. Suo, W. Hong, Z. Ren, C. F. Guo, *Adv. Mater.* **2019**, *31*, 1902955.

[37] A. Bele, C. Tugui, M. Asandulesa, D. Ionita, L. Vasiliu, G. Stiubianu, M. Iacob, C. Racles, M. Cazacu, *Smart Mater. Struct.* **2018**, *27*, 105005.

[38] S. Michel, B. T. T. Chu, S. Grimm, F. A. Nüesch, A. Borgschulte, D. M. Opris, *J. Mater. Chem.* **2012**, *22*, 20736.

[39] A. Chortos, E. Hajiesmaili, J. Morales, D. R. Clarke, J. A. Lewis, *Adv. Funct. Mater.* **2019**, *30*, 1907375.

[40] J.-E. Lim, S.-M. Lee, S.-S. Kim, T.-W. Kim, H.- W. Koo, H.-K. Kim, *Sci. Rep.* **2017**, *7*, 14685.

[41] H. Wei, K. Li, W. G. Liu, H. Meng, P. X. Zhang, C. Y. Yan, *Adv. Eng. Mater.* **2017**, *19*, 1700341.

[42] B. Fasolt, M. Hodgins, G. Rizzello, S. Seelecke, *Sens. Actuators, A* **2017**, *265*, 10.

[43] S. Yoon, H.-K. I. Kim, *Surf. Coat. Technol.* **2020**, *384*, 125308.

[44] J. Liang, K. Tong, Q. Pei, *Adv. Mater.* **2016**, *28*, 5986.

[45] P. He, J. Cao, H. Ding, C. Liu, J. Neilson, Z. Li, I. A. Kinloch, B. Derby, *ACS Appl. Mater. Interfaces* **2019**, *11*, 32225.

[46] D. G. Papageorgiou, I. A. Kinloch, R. J. Young, *Prog. Mater. Sci.* **2017**, *90*, 75.

[47] A. R. Gilbert, S. W. Kantor, *J. Polym. Sci.* **1959**, *40*, 35.

[48] C. Tugui, V. Tiron, M. Dascalu, L. Sacarescu, M. Cazacu, *Eur. Polym. J.* **2019**, *120*, 109243.

[49] M. V. Circu, Y. S. Ko, A. C. Gerecke, D. M. Opris, *Macromol. Mater. Eng.* **2014**, *299*, 1126.

[50] A. Georgopoulou, S. Michel, B. Vanderborght, F. Clemens, *Sens. Actuators, A* **2021**, *318*, 112433.

[51] J. Hughes, F. Iida, *Sensors* **2018**, *18*, 3822.

[52] Z. Wang, X. Guan, H. Huang, H. Wang, W. Lin, Z. Peng, *Adv. Funct. Mater.* **2019**, *29*, 1807569.

[53] T. Stockinger, D. Wirthl, G. Mao, M. Drack, R. Pruckner, S. Demchyshyn, M. Steiner, F. Egger, U. Müller, R. Schwödiauer, S. Bauer, N. Arnold, M. Kaltenbrunner, *Adv. Mater.* **2021**, *33*, 2102736.

[54] R. S. Diteesawat, A. Fishman, T. Helps, M. Taghavi, J. Rossiter, *Front. Robot. AI* **2020**, *7*, 557624.

[55] W. Guo, P. Zheng, X. Huang, H. Zhuo, Y. Wu, Z. Yin, Z. Li, H. Wu, *ACS Appl. Mater. Interfaces* **2019**, *11*, 8567.

[56] N. Matsuhisa, D. Inoue, P. Zalar, H. Jin, Y. Matsuba, A. Itoh, T. Yokota, D. Hashizume, T. Someya, *Nat. Mater.* **2017**, *16*, 834.

[57] F. B. Albuquerque, H. R. Shea, *Proc. SPIE* **2021**, *11587*, 115871B.

[58] P. Caspari, S. J. Dünki, F. A. Nüesch, D. M. Opris, *J. Mater. Chem. C* **2018**, *6*, 2043.

[59] G. Kovacs, S. M. Ha, S. Michel, R. Pelrine, Q. Pei, *Proc. SPIE* **2008**, *6927*, 69270X.

[60] G. Kovacs, P. Lochmatter, M. Wissler, *Smart Mater. Struct.* **2007**, *16*, S306.

[61] A. M. Wemyss, C. Ellingford, Y. Morishita, C. Bowen, C. Wan, *Angew. Chem., Int. Ed.* **2021**, *60*, 13725.

[62] J. Ekeocha, C. Ellingford, M. Pan, A. M. Wemyss, C. Bowen, C. Wan, *Adv. Mater.* **2021**, *33*, 2008052.

[63] F. M. Smits, *Bell Syst. Tech. J.* **1958**, *37*, 711.